Chemical Science

ROYAL SOCIETY OF CHEMISTRY

EDGE ARTICLE

View Article Online
View Journal | View Issue

Cite this: *Chem. Sci.*, 2025, **16**, 5283

All publication charges for this article have been paid for by the Royal Society of Chemistry

Stable self-powered X-ray detection with a low detection limit using a green halide hybrid perovskite ferroelectric crystal†

Yueying Wang,[a] Qianwen Guan,[b] Zeng-Kui Zhu,*[a] Huang Ye,[b] Hang Li,[b] Ying Zeng,[a] Panpan Yu,[a] Huawei Yang,[a] Wenhui Wu[a] and Junhua Luo *[ab]

Received 6th September 2024
Accepted 1st February 2025

DOI: 10.1039/d4sc06049k

rsc.li/chemical-science

Lead halide hybrid perovskite ferroelectrics show great potential in the field of self-powered X-ray detection due to their excellent X-ray absorption, high carrier mobility, large carrier lifetime, and interesting ferroelectricity. Nonetheless, the toxicity of lead raises concerns regarding safety for humans and the environment, which limits their practical applicability. Herein, we successfully realized stable self-powered X-ray detection with a low detection limit using a lead-free halide hybrid perovskite ferroelectric crystal, $[H_2mdap]BiBr_5$ (**1**, H_2mdap = *N*-methyl-1,3-diaminopropanium), driven by the switchable spontaneous polarization (P_s). Specifically, a remarkable switchable ferroelectric-photovoltaic (FE-PV) effect and excellent open-circuit photovoltage under X-ray irradiation endow **1** with a self-powered detection capability. Strikingly, the **1** detector shows a relatively high sensitivity of 79.0 μC Gy^{-1} cm^{-2} under 22 keV X-rays and achieves a low detection limit of 28 nGy s^{-1} at zero bias, much lower than that of the regular medical diagnosis (~5.5 μGy s^{-1}). Additionally, **1** also shows good operational stability, which may benefit from a stable structure and high activation energy (E_a). This study successfully demonstrates self-powered X-ray detection in 1D lead-free ferroelectric materials, which opens up new possibilities for safe and stable X-ray detection.

Introduction

The transformation of X-ray radiation into electrical signals using direct X-ray detectors holds significant value in areas such as wearable dosimeters, medical diagnostics, security checks, and scientific investigation.[1–4] However, most X-ray detectors operate at high external electric fields, often leading to operational instability, high energy consumption, and bulky overall circuitry. Recently, self-powered X-ray detectors without the requirement for external electric fields have attracted interest.[5–9] In conventional strategies, photogenerated carriers are separated and transmitted through p–n heterojunctions and p–i–n devices with a built-in electric field to enable self-powered detection.[10–13] However, these approaches are plagued by issues such as interface engineering and complicated experimental procedures. Comparatively, as a much simpler technology, ferroelectric materials exhibit the ferroelectric-photovoltaic (FE-PV) effect directed by intrinsic spontaneous polarization (P_s), which can separate and transmit photogenerated carriers independently and make them well-suited for developing next-generation radiation devices with X-ray detection at 0 V bias.[14,15] Recently, lead halide perovskite ferroelectrics have demonstrated considerable potential as X-ray detectors, thanks to their excellent X-ray absorption, large carrier mobility-lifetime ($\mu\tau$) products, low fabrication cost, and interesting ferroelectricity.[16–18] For instance, the $(CH_3OC_3H_9N)_2CsPb_2Br_7$ ferroelectric single crystal (SC) shows a considerable sensitivity under zero bias;[19] the $(NPA)_2(EA)_2Pb_3Br_{10}$ ferroelectric SC presents a detection limit of 83.4 nGy s^{-1} at 0 V bias.[20] Despite great progress, the toxicity of lead to some extent has prevented their practical applications toward green and sustainable competitors. Taking lead toxicity issues into account, the development of novel lead-free hybrid perovskite ferroelectrics is imperative for self-powered X-ray detection.

It is worth noting that bismuth halide perovskites (BHPs) are lead-free and environmentally friendly, have excellent phase stability, and possess good photophysical properties. Indeed, a wide variety of BHPs are available for self-powered X-ray detection that performs impressively as exemplified by $(R\text{-MPA})_4AgBiI_8$ (85 nGy s^{-1}), (4-AMP)BiI_5 (482 nGy s^{-1}), *etc.*[21–25] However, investigations on BHP ferroelectric materials have rarely been conducted in the X-ray region for self-powered detection, with only one example, $(HDA)BiI_5$, which shows a high sensitivity of 170.7 μC Gy^{-1} cm^{-2} and a low detection limit of 266 nGy s^{-1} at 0 V bias, to date.[26] Furthermore, the issue

[a]*College of Chemistry and Materials, School of Chemical Engineering, Key Laboratory of Fluorine and Silicon for Energy Materials and Chemistry of Ministry of Education, Jiangxi Normal University Nanchang, Jiangxi 330022, P. R. China*

[b]*State Key Laboratory of Structural Chemistry Fujian Institute of Research on the Structure of Matter, Chinese Academy of Sciences, Fuzhou, Fujian 350002, P. R. China. E-mail: zkzhu@jxnu.edu.cn; jhluo@fjirsm.ac.cn*

† Electronic supplementary information (ESI) available. See DOI: https://doi.org/10.1039/d4sc06049k

of ion migration poses a significant challenge for perovskite materials, particularly in detector applications where it leads to current drift and increases the noise current.[27–29] Experimental evidence has illustrated that low-dimensional perovskites effectively suppress ion migration.[30,31] Therefore, it is a rewarding frontier to exploit self-powered X-ray detection in low-dimensional BHP ferroelectrics.

Herein, we successfully realized self-powered X-ray detection with a low detection limit based on "green" BHP ferroelectrics. Specifically, exploiting the FE-PV effect of the BHP ferroelectric, $[H_2mdap]BiBr_5$ (**1**, H_2mdap = *N*-methyl-1,3-diaminopropanium), presents a remarkable open-circuit photovoltage of 0.50 V along its polar axis. Moreover, a large $\mu\tau$ product value (3.2×10^{-4} cm^2 V^{-1}) under X-ray irradiation verifies its remarkable charge transport ability. Specifically, benefiting from these merits, the **1** SC detector exhibits outstanding self-powered X-ray detection performance with relatively high sensitivity and a low detection limit of 28 nGy s^{-1} at zero bias, which is lower than those of most Bi-based X-ray detector materials and also over 196-fold lower than the value of the typical medical diagnosis (5.5 μGy s^{-1}). **1** also shows a low dark current drift (I_{drift}) of 4.66×10^{-7} nA cm^{-1} s^{-1} V^{-1}, exhibiting good operational stability. These results highlight the way to dramatically decrease the detection limit of self-powered BHP-based X-ray detectors.

Results and discussion

The reported BHP ferroelectric **1** was synthesized from stoichiometric Bi_2O_3 and H_2mdap in a saturated hydrobromic acid solution[32] and adopted the noncentrosymmetric orthorhombic space group $Pna2_1$ in the ferroelectric phase (Fig. 1a) and centrosymmetric space group *Pnma* in the paraelectric phase (Fig. S1, ESI†), which belongs to one of the reported 88 species of ferroelectric phase transitions deduced through the Aizu notation of *mmmFmm*2. Its basic 1D, ABX_5-type perovskite structure consists of an inorganic zigzag chain formed by $\{BiBr_5\}_n$ and the $[H_2mdap]^{2+}$ cations are located in the inorganic framework. A pair of amino groups in $[H_2mdap]^{2+}$ cations are tightly linked with the inorganic structure, creating sturdy N–H···Br hydrogen bonds (Fig. S2, ESI†), which strengthens the stability of the structure.[33]

Large yellow crystals (*i.e.*, 13 × 5 × 0.5 mm^3) were obtained *via* a gradual process of solvent evaporation (Fig. 1b and c). The purity of the samples was confirmed through powder X-ray diffraction (Fig. 1d). As shown in Fig. S3 (ESI),† the test result shows that **1** is environmentally stable after being stored in ambient air for 1 month and 3 months. The thermogravimetric analysis shows that **1** also has ultrahigh thermal stability up to 580 K (Fig. S4, ESI†). Moreover, we measured the *P*–*E* hysteresis loop along the crystallographic *c*-axis direction, and the P_s value of **1** reaches ~3.1 μC cm^{-2} (Fig. S5, ESI†). Additionally, ferroelectric materials are distinguished by their ability to reversibly alter the orientation of the P_s by applying an external electric field, thereby providing a practical means for controlling the P_s-based photovoltaic currents. To explore the link between ferroelectricity and self-powered behaviors, we realized the reversal of the optical voltage direction through the poling electric field's directional change. When exposed to 404 nm light, the clear P_s-linked FE-PV effect of switchable open-circuit optical voltage (V_{OC}) is noticeable with its value of ~0.20 V (Fig. 1e). The changeable V_{OC} signal reveals a complex

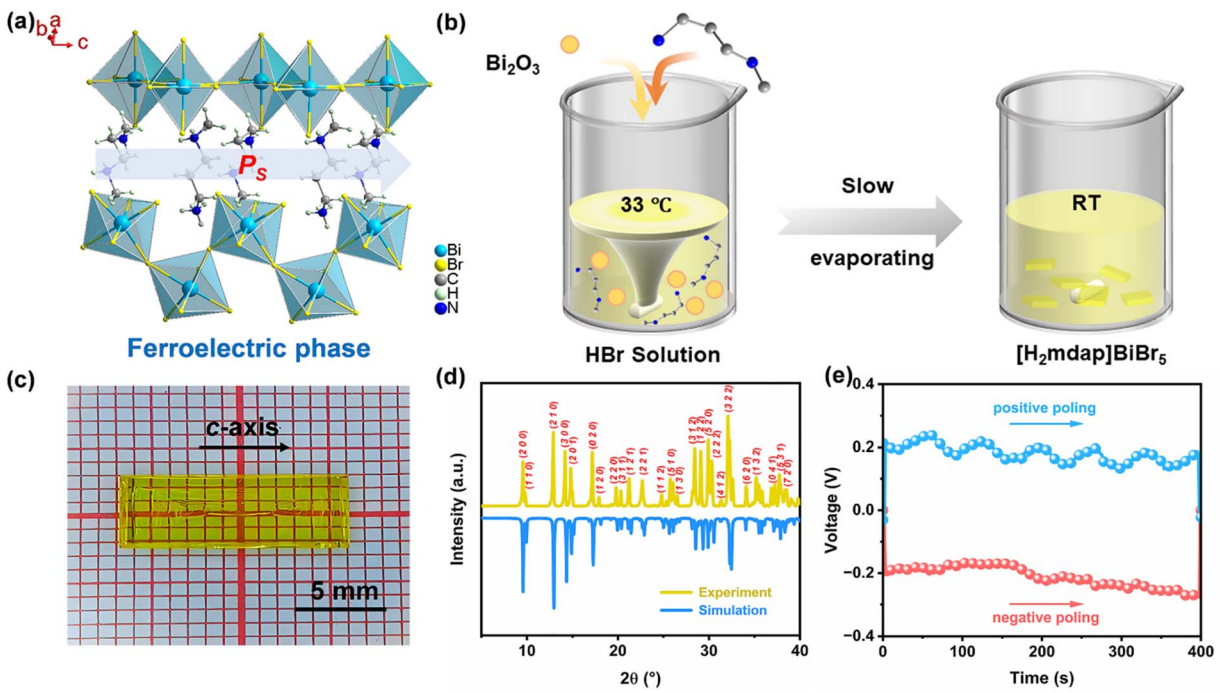

Fig. 1 (a) The crystal structure of **1** in the ferroelectric phase; (b) schematic for the growth of the **1** crystal; (c) a photograph for the **1** SC; (d) the experimental and simulated powder XRD patterns; (e) *V*–*t* curves along the *c*-axis, measured after positive and negative polings.

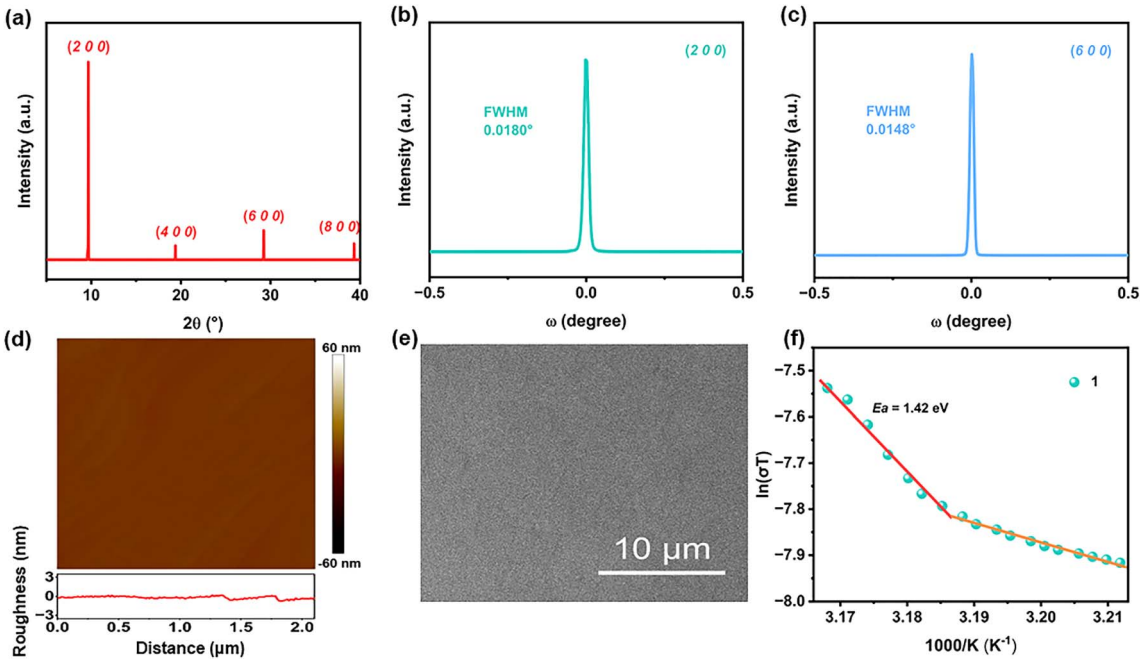

Fig. 2 (a) XRD scan of the top facet of the **1** SC; (b and c) high-resolution XRD rocking curves for the diffraction peaks at (2 0 0) and (6 0 0), respectively; (d) AFM image of the **1** SC; (e) SEM image of the **1** SC; (f) the variable temperature conductivity measurement on **1**.

connection between the FE-PV effect and the inherent electric field in ferroelectrics, aiding in the segregation and transfer of photon-generated carriers, thereby hinting at self-powered detection capabilities.

Moreover, the crystal's quality is pivotal in determining X-ray detection performance. The X-ray scan of the top facet of the **1** SC shows only (h 0 0) diffraction peaks (Fig. 2a), confirming its well-oriented single-crystalline lattice and good crystallinity. A more detailed rocking-curve analysis shows that a very narrow full width at half maximum (FWHM) of only 0.0180° and 0.0148° for the (2 0 0) and (6 0 0) peaks is obtained (Fig. 2b and c), lower than those of many reported X-ray detectors, including high-quality $MA_3Bi_2I_9$ (0.024° at the (0 0 6) peak)[34] and $MAPbI_3$ (0.0414° at the (2 0 0) peak).[35] Additionally, the atomic force microscope (AFM) measurement (Fig. 2d) and the scanning electron microscope (SEM) measurement (Fig. 2d) were conducted on the **1**'s (h 0 0) plane which shows that **1** has a very smooth and flat morphology, further confirming the high crystal quality, prone to photogenerated carriers' transport in direct X-ray detectors.

Furthermore, based on the I–V curves ranging from −4 to 4 V, a relatively high bulk resistivity (ρ) is calculated to be 2.53×10^{10} Ω cm^{-1} (Fig. S6, ESI†), which is comparable to those of many lead-free halide perovskites, such as $(MA)_3Bi_2I_9$ (3.74×10^{10} Ω cm^{-1}),[34] $(I\text{–}C_4H_8NH_3)_4AgBiI_8$ (3.04×10^{10} Ω cm^{-1}),[36] and commercial CdZnTe (10^{10} Ω cm^{-1}),[37] with its orders of magnitude greater than those of 3D lead halide perovskite SCs (10^7–10^8 Ω cm^{-1}).[38,39] This high resistivity would permit an extremely low dark current, which is crucial for stable high-performance X-ray detection.[40] We also measured the variable temperature conductivity to extract the activation energy E_a based on the Nernst–Einstein relation:[41]

$$\sigma(T) = \left(\frac{\sigma_0}{T}\right)\exp\left(-\frac{E_a}{K_B T}\right) \quad (1)$$

where σ signifies the conductivity at a given temperature (T), σ_0 represents a constant, and K_B is the Boltzmann constant. As shown in Fig. 2f, the E_a is calculated to be 1.42 eV, which is greater than that of the previously reported Pb-based perovskite devices such as $MAPbI_3$ (E_a = 0.54 eV)[34] and $MAPbBr_3$ (E_a = 0.168 eV).[42] Such a high E_a value benefits from the strong hydrogen bonding of the double amino groups, which will enhance the perovskite X-ray detector's operational stability.

What's more, self-powered X-ray detection was executed on the **1** detector along the polar axis (c-axis) as demonstrated in Fig. 3a (Fig. S7, ESI†). To accurately determine the X-ray photon absorption capacity of **1**, the absorption spectra of **1** as a function of photon energies were obtained using the photo cross-section database.[43] In Fig. 3b, the absorption coefficient of **1** is shown to be higher than that of Si and comparable to that of traditional semiconductors α-Se and the $MA_3Bi_2I_9$ SC, indicating its good X-ray attenuation ability, which guarantees **1** to be applied in direct X-ray detection. Specifically, for 50 keV hard X-ray photons, a 1.5 mm-thick **1** SC can absorb ≈ 92% of incident photons, much better than the ratio (≈15%) for Si (Fig. S8, ESI†), hence enabling the charge carriers to be collected more easily. Furthermore, efficient charge collection is also crucial for a high-performance detector, which is determined by the high $\mu\tau$ product according to the standard Hecht's equation:[44]

$$I = \frac{I_0 \mu\tau V}{L^2}\left[1 - \exp\left(-\frac{L^2}{\mu\tau\ V}\right)\right] \quad (2)$$

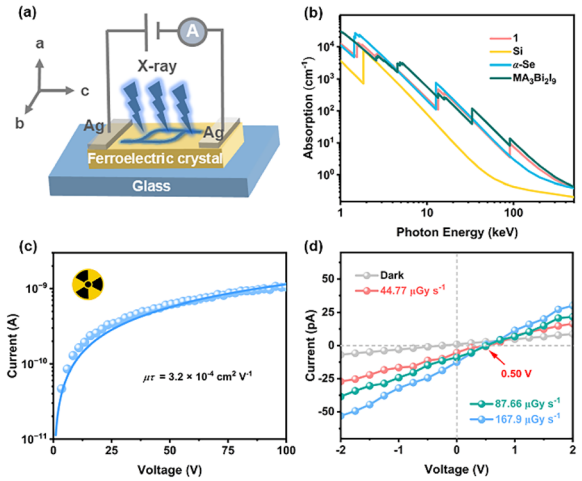

Fig. 3 (a) The device fabrication of the Ag |**1** SC| Ag with the electrode direction parallel to the *c*-axis; (b) calculated absorption spectra of **1**, Si, α-Se, and $MA_3Bi_2I_9$; (c) Bias-dependent photoconductivity of **1**; (d) *I*–*V* curves of the **1** device along the *c*-axis in the dark and under X-ray irradiation.

In the equation, I, I_0, V, and L denote the photocurrent, the saturated photocurrent, the applied bias, and the thickness of the material, respectively. The X-ray detector based on **1** shows a $\mu\tau$ value up to 3.2×10^{-4} cm^2 V^{-1} (Fig. 3c), which is equivalent to the values for lead-free perovskite X-ray detectors, such as (*R*-MPz)$_6$Bi$_3$I$_{21}\cdot$6H$_2$O (3.24×10^{-4} cm^2 V^{-1}),[45] (BAH)BiI$_4$ (1.95×10^{-4} cm^2 V^{-1}),[46] and (*R*-MPA)$_4$AgBiI$_8$ (2.2×10^{-5} cm^2 V^{-1}),[21] but much higher than that of the commercial α-Se film ($\approx 10^{-7}$ cm^2 V^{-1}).[47] Considering **1**'s ferroelectric phase at room temperature, it is expected to exhibit an obvious FE-PV effect along the polarization direction (*c*-axis) in the *I*–*V* measurements. Under X-ray radiation, a remarkable FE-PV effect is noted with an open-circuit voltage of 0.50 V (Fig. 3d), which lays the foundation for spontaneously separating and transporting photogenerated carriers, thereby enabling **1** with the capacity for self-powered X-ray detection. By combining excellent X-ray absorption capability, a large mobility-lifetime product, and a strong FE-PV effect, the **1** SC is very promising for use in high-performance self-powered X-ray detection.

As a result, we test the X-ray detection performance of **1**. Here, an Amptek Mini-X2 X-ray tube with a silver target (maximum power 4 W) is used as the X-ray source. The X-ray energy is up to 50 keV and the peak intensity is at 22 keV (Fig. S9a, ESI†). As shown in Fig. 4a, owing to the significant FE-PV effect induced by the spontaneous electric polarization, the **1** detector exhibits its excellent response to X-ray irradiation even at 0 V bias, with a fitting sensitivity of 79.0 μC Gy^{-1} cm^{-2} (Fig. 4c), four times higher than that of the commercial α-Se film detector (20 μC Gy^{-1} cm^{-2} under 2000 V) and higher than those of many reported self-powered X-ray detectors, including (4-AMP)BiI$_5$ (66.84 μC Gy^{-1} cm^{-2}),[22] (*R*-PPA)BiI$_5$ (31 μC Gy^{-1} cm^{-2}),[48] *etc.* To the best of our knowledge, **1** successfully realizes the self-powered X-ray detection in 1D BHP ferroelectrics, showing its potential for future practical application. Furthermore, with the increase of the applied bias, the photocurrent density increases almost linearly with increasing X-ray dose rates (Fig. 4b and S10, ESI†). Additionally, the sensitivity can reach the highest value of 2618.7 μC Gy^{-1} cm^{-2} at −80 V bias, which surpasses those of most 1D X-ray detectors (Table S1, ESI†), showing that it's a promising material for X-ray detection. Moreover, such a high value exceeds the theoretical sensitivity of 24.6 and 2.1 μC Gy^{-1} cm^{-2} at a maximum X-ray energy of 50 keV and a peak intensity of 22 keV, respectively.[49] This is likely due to photoconductive gain, a widespread

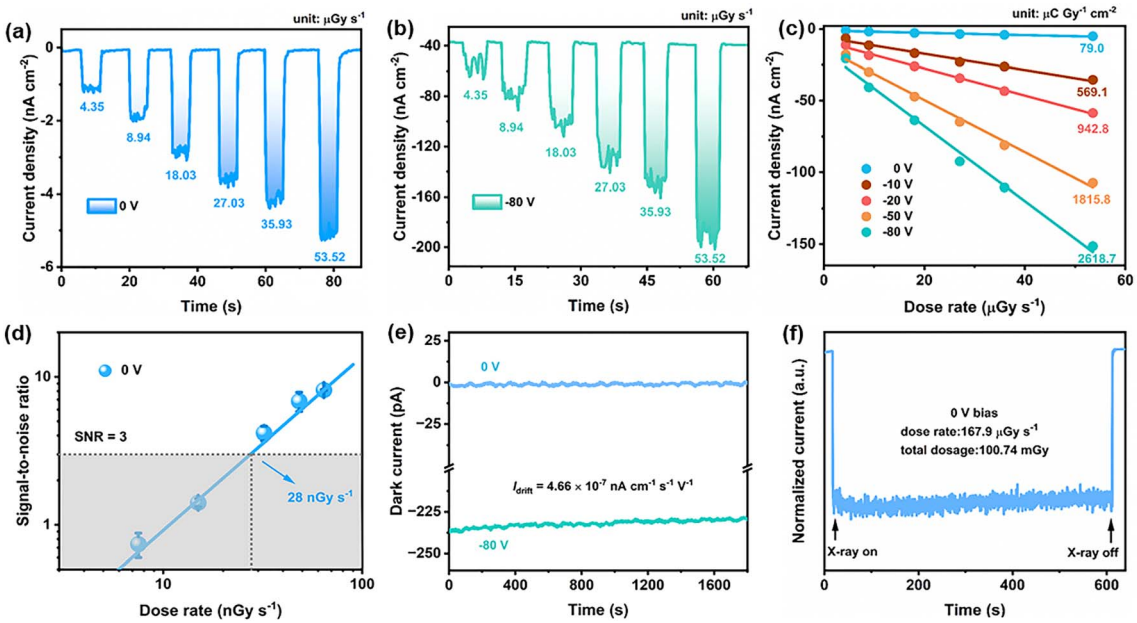

Fig. 4 (a and b) Photoresponses of the **1** detector to X-rays at increased dose rates at 0 and −80 V bias, respectively; (c) X-ray photocurrent density as a function of the dose rate; (d) X-ray dose rate dependent SNR at zero bias; (e) the dark current drift at −80 V bias; (f) the stable photoresponse of the **1** device resisting X-ray irradiation.

phenomenon, and is beneficial for increasing the sensitivity of X-ray detectors.[40,50–52]

In addition, under 0 V bias, the SNR rates for **1** were further calculated. According to the International Union of Pure and Applied Chemistry (IUPAC), the dose rate that generates an SNR of three is regarded as the lowest detection limit.[40] **1** still has a good photoresponse at a low dose of 4.35 μGy s^{-1}, according to the plot of the photocurrent density *versus* the dose ratio, suggesting its ability to detect weak X-rays. Therefore, we measured its photocurrent at a lower X-ray dose rate (Fig. S11, ESI†). At 0 V bias, a low detection limit (28 nGy s^{-1}) of **1** is 196 times lower than the regular medical diagnosis of 5.5 μGy s^{-1} (Fig. 4d).[53] The detection limit of **1** under −10 to −80 V was also calculated with detection limits of 749, 1989, 2384, and 3511 nGy s^{-1}, respectively (Fig. S12, ESI†), all of which exceed the value at 0 V bias, showing that the detection limit can be greatly reduced in self-powered mode. Then, to evaluate the operating stability of **1**, the I_{drift} under −80 V bias is further analyzed (Fig. 4e). The value of I_{drift} (4.66×10^{-7} nA cm^{-1} s^{-1} V^{-1}) is lower than that of 1D (4-AMP)BiI_5 (about 1.51×10^{-5} nA cm^{-1} s^{-1} V^{-1}, 50 V),[22] 2D (*R*-MPA)$_4AgBiI_8$ (about 10^{-3} nA cm^{-1} s^{-1} V^{-1}, 50 V),[21] and 3D perovskites, including $MAPbI_3$ (about 10^{-4} nA cm^{-1} s^{-1} V^{-1}, 100 V cm^{-1})[54] and $MAPbBr_3$ (about 10^{-3} nA cm^{-1} s^{-1} V^{-1}, 20 V cm^{-1}),[52] showing its good operational stability, probably owing to the 1D inorganic framework and the strong hydrogen bonds in **1**. Then, the high dose stability of **1** was investigated, showing that **1** retained stability at total X-ray doses of 100.74 mGy (Fig. 4f), thereby highlighting its relatively high radiation stability.

Conclusions

In summary, we have successfully explored the ferroelectric in the class of 1D BHPs, $[H_2mdap]BiBr_5$ (**1**), toward relatively "green" self-powered X-ray detection. Exploiting the FE-PV effect, the **1** device demonstrates remarkable sensitivity. It achieves a low detection limit of 28 nGy s^{-1} at zero bias, surpassing most Bi-based X-ray detector materials and the typical medical diagnosis (~5.5 μGy s^{-1}). Furthermore, the **1** SC detector shows a low I_{drift} of 4.66×10^{-7} nA cm^{-1} s^{-1} V^{-1}, exhibiting good operational stability, which may benefit from a stable structure and high activation energy (E_a, 1.42 eV). This study introduces a novel approach to preparing self-powered X-ray detectors based on the FE-PV effect of ferroelectric SC materials. In the future, it will continue to develop on this basis, such as the manufacture of BHP-based ferroelectric thin-film devices for X-ray detection.

Data availability

The data supporting the findings of this study are available on request from the corresponding author, [Junhua Luo], upon reasonable request.

Author contributions

Y. Wang prepared the samples and wrote the manuscript. H. Yang, W. Wu, and Y. Wang investigated the photoelectric properties. Q. Guan, H. Ye, H. Li, Y. Zeng, and P. Yu provided suggestions for the project. Z.-K. Zhu and J. Luo designed and directed this project. All the authors discussed and commented on the manuscript.

Conflicts of interest

There are no conflicts to declare.

Acknowledgements

This work was financially supported by the National Natural Science Foundation of China (22435005, 22193042, 22201284, 22305105, 22405108, 22175177, 22125110, and U21A2069), the Key Research Program of Frontier Sciences of the Chinese Academy of Sciences (ZDBS-LY-SLH024), the National Key Research and Development Program of China (2019YFA0210402), the Natural Science Foundation of Fujian Province (2023J05076), the Natural Science Foundation of Jiangxi Province (20224BAB213003 and 20232BAB213020), the Jiangxi Provincial Education Department Science and Technology Research Foundation (GJJ2200384), and the Graduate Innovation Fund Project of Jiangxi Provincial Department of Education (YC2024-S266).

Notes and references

1 H. Li, C. f. Wang, Q. f. Luo, C. Ma, J. Zhang, R. Zhao, T. Yang, Y. Du, X. Chen, T. Li, X. Liu, X. Song, Y. Yang, Z. Yang, S. Liu, Y. Zhang and K. Zhao, *Adv. Funct. Mater.*, 2024, **34**, 2407693.
2 Y. Li, Y. Lei, H. Wang and Z. Jin, *Nano-Micro Lett.*, 2023, **15**, 128.
3 Y. Wu, J. Feng, Z. Yang, Y. Liu and S. Liu, *Adv. Sci.*, 2023, **10**, 2205536.
4 X. He, Y. Deng, D. Ouyang, N. Zhang, J. Wang, A. A. Murthy, I. Spanopoulos, S. M. Islam, Q. Tu, G. Xing, Y. Li, V. P. Dravid and T. Zhai, *Chem. Rev.*, 2023, **123**, 1207–1261.
5 J. H. Heo, J. K. Park, Y. M. Yang, D. S. Lee and S. H. Im, *iScience*, 2021, **24**, 102927.
6 H. Li, X. Liu, T. Yang, C. Ma, Y. Du, P. Xu, L. Zhang, X. Song, Q. Cui, S. Zhao, Z. Yang, S. Liu, S. Jin and K. Zhao, *ACS Energy Lett.*, 2024, **9**, 64–74.
7 N. Li, Y. Li, S. Xie, J. Wu, N. Liu, Y. Yu, Q. Lin, Y. Liu, S. Yang, G. Lian, Y. Fang, D. Yang, Z. Chen and X. Tao, *Angew. Chem., Int. Ed.*, 2023, **62**, e202302435.
8 J. Tan, X. Gao, X. Huang, P. Wangyang, H. Sun, D. Yang and T. Zeng, *J. Mater. Sci.: Mater. Electron.*, 2023, **34**, 1199.
9 Z.-K. Zhu, J. Wu, P. Yu, Y. Zeng, R. Li, Q. Guan, H. Dai, G. Chen, H. Yang, X. Liu, L. Li, C. Ji and J. Luo, *Adv. Funct. Mater.*, 2024, **34**, 2409857.
10 X. Zhang, T. Zhu, C. Ji, Y. Yao and J. Luo, *J. Am. Chem. Soc.*, 2021, **143**, 20802–20810.
11 J. Yan, F. Gao, Y. Tian, Y. Li, W. Gong, S. Wang, H. Zhu and L. Li, *Adv. Opt. Mater.*, 2022, **10**, 2200449.
12 M. Girolami, F. Matteocci, S. Pettinato, V. Serpente, E. Bolli, B. Paci, A. Generosi, S. Salvatori, A. D. Carlo and D. M. Trucchi, *Nano-Micro Lett.*, 2024, **16**, 182.

13 H. Tsai, F. Liu, S. Shrestha, K. Fernando, S. Tretiak, B. Scott, D. T. Vo, J. Strzalka and W. Nie, *Sci. Adv.*, 2020, **6**, eaay0815.
14 A. B. Swain, M. Rath, P. P. Biswas, M. S. R. Rao and P. Murugavel, *APL Mater.*, 2019, **7**, 011106.
15 Y. Peng, X. Liu, Z. Sun, C. Ji, L. Li, Z. Wu, S. Wang, Y. Yao, M. Hong and J. Luo, *Angew. Chem., Int. Ed.*, 2020, **59**, 3933–3937.
16 C. Ji, S. Wang, Y. Wang, H. Chen, L. Li, Z. Sun, Y. Sui, S. Wang and J. Luo, *Adv. Funct. Mater.*, 2020, **30**, 1905529.
17 Z. Zhu, H. Chen, B. Zhao, W. Huang, Q. Lin, X. Yu and Y. Li, *Appl. Phys. Lett.*, 2023, **122**, 163301.
18 Y. Jiang, C. Zhang, Z.-K. Zhu, J. Wu, P. Yu, Y. Zeng, H. Ye, H. Dai, R. Li, Q. Guan, G. Chen, H. Yang and J. Luo, *Angew. Chem., Int. Ed.*, 2024, **63**, e202407305.
19 C. Ji, Y. Li, X. Liu, Y. Wang, T. Zhu, Q. Chen, L. Li, S. Wang and J. Luo, *Angew. Chem., Int. Ed.*, 2021, **60**, 20970–20976.
20 Y. Ma, W. Li, Y. Liu, W. Guo, H. Xu, S. Han, L. Tang, Q. Fan, J. Luo and Z. Sun, *ACS Cent. Sci.*, 2023, **9**, 2350–2357.
21 J. Wu, S. You, P. Yu, Q. Guan, Z.-K. Zhu, Z. Li, C. Qu, H. Zhong, L. Li and J. Luo, *ACS Energy Lett.*, 2023, **8**, 2809–2816.
22 S. You, P. Yu, T. Zhu, C. Lin, J. Wu, Z.-K. Zhu, C. Zhang, Z. Li, C. Ji and J. Luo, *Adv. Funct. Mater.*, 2024, **34**, 2310916.
23 Z.-K. Zhu, T. Zhu, S. You, P. Yu, J. Wu, Y. Zeng, Q. Guan, Z. Li, C. Qu, H. Zhong, L. Li and J. Luo, *Small*, 2023, **20**, 2307454.
24 W. Guo, H. Xu, Q. Fan, P. Zhu, Y. Ma, Y. Liu, X. Zeng, J. Luo and Z. Sun, *Adv. Opt. Mater.*, 2024, **12**, 2303291.
25 D. Fu, Y. Ma, Z. Chen, Z. Hou and J. Luo, *Adv. Opt. Mater.*, 2024, **12**, 2400193.
26 D. Fu, Y. Ma, S. Wu, L. Pan, Q. Wang, R. Zhao, X. M. Zhang and J. Luo, *InfoMat*, 2024, **6**, e12602.
27 X. Xiao, J. Dai, Y. Fang, J. Zhao, X. Zheng, S. Tang, P. N. Rudd, X. C. Zeng and J. Huang, *ACS Energy Lett.*, 2018, **3**, 684–688.
28 Y. Zhang, Y. Liu, Z. Xu, Z. Yang and S. Liu, *Small*, 2020, **16**, 2003145.
29 B. Zhang, Z. Xu, C. Ma, H. Li, Y. Liu, L. Gao, J. Zhang, J. You and S. Liu, *Adv. Funct. Mater.*, 2022, **32**, 2110392.
30 Y. Yuan and J. Huang, *Acc. Chem. Res.*, 2016, **49**, 286–293.
31 Y. Lin, Y. Bai, Y. Fang, Q. Wang, Y. Deng and J. Huang, *ACS Energy Lett.*, 2017, **2**, 1571–1572.
32 Q. Chen, H. Jiang, Y. Fan, Z. Li, H. Ye, Y. Yao, S. Chen, C. Ji, S. Zhang and J. Luo, *Adv. Funct. Mater.*, 2023, **33**, 2213964.
33 N. K. Tailor, A. Mahapatra, A. Kalam, M. Pandey, P. Yadav and S. Satapathi, *Phys. Rev. Mater.*, 2022, **6**, 045401.
34 Y. Liu, Z. Xu, Z. Yang, Y. Zhang, J. Cui, Y. He, H. Ye, K. Zhao, H. Sun, R. Lu, M. Liu, M. G. Kanatzidis and S. Liu, *Matter*, 2020, **3**, 180–196.
35 J. Wu, L. Wang, A. Feng, S. Yang, N. Li, X. Jiang, N. Liu, S. Xie, X. Guo, Y. Fang, Z. Chen, D. Yang and X. Tao, *Adv. Funct. Mater.*, 2022, **32**, 2109149.
36 Z. Xu, H. Wu, D. Li, W. Wu, L. Li and J. Luo, *J. Mater. Chem. C*, 2021, **9**, 13157–13161.
37 K. Kim, S. Kim, J. Hong, J. Lee, T. Hong, A. E. Bolotnikov, G. S. Camarda and R. B. James, *J. Appl. Phys.*, 2015, **117**, 145702.
38 G. Maculan, A. D. Sheikh, A. L. Abdelhady, M. I. Saidaminov, M. A. Haque, B. Murali, E. Alarousu, O. F. Mohammed, T. Wu and O. M. Bakr, *J. Phys. Chem. Lett.*, 2015, **6**, 3781–3786.
39 D. Shi, V. Adinolfi, R. Comin, M. Yuan, E. Alarousu, A. Buin, Y. Chen, S. Hoogland, A. Rothenberger, K. Katsiev, Y. Losovyj, X. Zhang, P. A. Dowben, O. F. Mohammed, E. H. Sargent and O. M. Bakr, *Science*, 2015, **347**, 519–522.
40 W. Pan, H. Wu, J. Luo, Z. Deng, C. Ge, C. Chen, X. Jiang, W.-J. Yin, G. Niu, L. Zhu, L. Yin, Y. Zhou, Q. Xie, X. Ke, M. Sui and J. Tang, *Nat. Photonics*, 2017, **11**, 726–732.
41 S. Yang, S. Chen, E. Mosconi, Y. Fang, X. Xiao, C. Wang, Y. Zhou, Z. Yu, J. Zhao, Y. Gao, F. D. Angelis and J. Huang, *Science*, 2019, **365**, 473–478.
42 S. Meloni, T. Moehl, W. Tress, M. Franckevicius, M. Saliba, Y. H. Lee, P. Gao, M. K. Nazeeruddin, S. M. Zakeeruddin, U. Rothlisberger and M. Graetzel, *Nat. Commun.*, 2016, **7**, 10334.
43 Y. Huang, L. Qiao, Y. Jiang, T. He, R. Long, F. Yang, L. Wang, X. Lei, M. Yuan and J. Chen, *Angew. Chem., Int. Ed.*, 2019, **58**, 17834–17842.
44 Y. C. Kim, K. H. Kim, D.-Y. Son, D.-N. Jeong, J.-Y. Seo, Y. S. Choi, I. T. Han, S. Y. Lee and N.-G. Park, *Nature*, 2017, **550**, 87–91.
45 X. Dong, T. Chen, J. Liang, L. Wang, H. Wu, Z. Xu, J. Luo and L.-N. Li, *Chin. J. Struct. Chem.*, 2024, **43**, 100256.
46 C. Ma, H. Li, M. Chen, Y. Liu, K. Zhao and S. Liu, *Adv. Funct. Mater.*, 2022, **32**, 2202160.
47 Y. Zhou, J. Chen, O. M. Bakr and O. F. Mohammed, *ACS Energy Lett.*, 2021, **6**, 739–768.
48 S. You, Z.-K. Zhu, S. Dai, J. Wu, Q. Guan, T. Zhu, P. Yu, C. Chen, Q. Chen and J. Luo, *Adv. Funct. Mater.*, 2023, **33**, 2303523.
49 W. Pan, Y. He, W. Li, L. Liu, K. Guo, J. Zhang, C. Wang, B. Li, H. Huang, J. Zhang, B. Yang and H. Wei, *Nat. Commun.*, 2024, **15**, 257.
50 K. Guo, W. Li, Y. He, X. Feng, J. Song, W. Pan, W. Qu, B. Yang and H. Wei, *Angew. Chem., Int. Ed.*, 2023, **62**, e202303445.
51 W.-G. Li, X.-D. Wang, Y.-H. Huang and D.-B. Kuang, *Adv. Mater.*, 2023, **35**, 2210878.
52 W. Wei, Y. Zhang, Q. Xu, H. Wei, Y. Fang, Q. Wang, Y. Deng, T. Li, A. Gruverman, L. Cao and J. Huang, *Nat. Photonics*, 2017, **11**, 315–321.
53 H. Wei and J. Huang, *Nat. Commun.*, 2019, **10**, 1066.
54 S. Yakunin, D. N. Dirin, Y. Shynkarenko, V. Morad, I. Cherniukh, O. Nazarenko, D. Kreil, T. Nauser and M. V. Kovalenko, *Nat. Photonics*, 2016, **10**, 585–589.